Inorg. Chem. **2003**, *42*, 4046–4056

Comparative Theoretical Investigation of the Vertical Excitation Energies and the Electronic Structure of $[Mo^{V}OCl_4]^{-}$: Influence of Basis Set and Geometry

Victor N. Nemykin* and Partha Basu*

Department of Chemistry and Biochemistry, Duquesne University, 600 Forbes Avenue, Pittsburgh, Pennsylvania 15282

Received December 20, 2002

The electronic structures, geometries, and vibration frequencies of the open-shell molybdenum(V) ion, $[MoOCl_4]^{-}$, have been calculated at the extended Hückel, semiempirical ZINDO/1, ZINDO/S, and PM3(tm), as well as ab initio and DFT theoretical levels. Electronic structure calculations suggest that the expected metal-fold orbital order can be satisfied only at the DFT level. The time-dependent density functional theory (TDDFT) approach has been used for the calculation of the vertical excitation energies in the UV–vis region with different basis sets, starting geometries, and exchange-correlation functionals. A good agreement between the predicted and the experimental electronic absorption and MCD spectra of the complex, $[MoOCl_4]^{-}$, was observed when the B3LYP and B3P86 exchange-correlation functionals were used with a full electron valence double-ζ with polarization basis set for the molybdenum and 6-311G(d) for all other atoms. Similar results were obtained when the LANL2DZ effective core potential for molybdenum atom and 6-31G(d) for all other atoms were used. The best absolute deviation of 0.13 and mean deviation of 0.01 eV were calculated for the bands in the UV–vis region by B3P86, while the results for the B3LYP exchange-correlation functional were less satisfactory. Compared to polarization functions, the inclusion of diffuse functions resulted in little improvement. The calculated excitations energies and charge-transfer band intensities are found to be sensitive to the Mo═O distance and O—Mo—Cl angle.

1. Introduction

Mononuclear molybdoenzymes are involved in the global cycling of nitrogen, sulfur, and arsenic. During the catalysis, the Mo-center cycles through +6, +5, and +4 oxidation states. While enzymes with +4 or +6 oxidation states have been characterized by crystallography, probing the +5 oxidation states relies on spectroscopic techniques, e.g., electron paramagnetic resonance, UV−vis spectroscopy, and magnetic circular dichroism (MCD). Discrete inorganic molecules have played a key role by serving as a vehicle for understanding more complex enzymatic systems.[1] To this end, several penta- and hexacoordinate Mo^{V}-complexes have been investigated that have provided valuable insight into the enzymatic active centers and their functions. In general, the spectroscopic results are interpreted using ligand field theory and ground state electronic structure calculations. While excited state calculations using quantum-chemical methods are yet to be applied to biomimetic molybdenum systems, such calculations have been reported for a number of molybdenum compounds.[2−4]

Among the available approaches for the calculation of vertical excitation energies, the configuration interaction methods (e.g., configuration interaction singles, CIS) and direct methods (e.g., time-dependent) are very common.[5] In the first approach, the CI matrix is diagonalized, and then, the differences between the eigenvalues of the CI matrix of the ground state configuration and various excited states are

* To whom correspondence should be addressed. E-mail: basu@duq.edu (P.B.).

(1) Jones, R. M.; Inscore, F. E.; Hille, R.; Kirk, M. L. *Inorg. Chem.* **1999**, *38*, 4963−4970. Helton, M. E.; Pacheco, A.; McMaster, J.; Enemark, J. H.; Kirk, M. L. *J. Inorg. Biochem.* **1999**, *80*, 227−233. Benson, N.; Farrar, J. A.; McEwan, A. J.; Thomson, M. J. *FEBS Lett.* **1992**, *307*, 169−172. Finnega, M. G.; Hilton, J.; Rajagopalan, K. V.; Johnson, M. K. *Inorg. Chem.* **1993**, *32*, 2616−2617.

(2) Nakai, H.; Morita, H.; Tomasello, P.; Nakatsuji, H. *J. Phys. Chem. A* **1998**, *102*, 2033−2043. Cotton, F. A.; Feng, X. *Inorg. Chem.* **1996**, *35*, 4921−4925.

(3) (a) Wen-Dan, C.; Guo-Cong, G.; Jin-Shun, H.; Jia-Xi, L. *Polyhedron* **1995**, *14*, 3649−3654. (b) Li, W.; Hong, M.; Cao, R.; Kang, B.; Liu, H. *J. Magn. Reson.* **1999**, *138*, 80−88. (c) Rodriguez, J. A. *J. Phys. Chem. B* **1997**, *101*, 7524−7534.

(4) Kim, W.-S.; Kaltsoyannis, N. *Inorg. Chem.* **1998**, *37*, 674−678. Miao, Q.; Adachi, H.; Tanaka, I.; Xin, X.-Q. *J. Phys. Chem. A* **1997**, *101*, 5818−5823.

10.1021/ic0262942 CCC: $25.00
Published on Web 06/05/2003

calculated. The CIS methods with the intermediate neglect of differential overlap (INDO) approximation, especially with Zerner's spectroscopic parametrization, has been applied in calculating vertical excitation energies of first and second row transition metal complexes.[6,7] Another semiempirical method, PM3-CIS,[8] has also been successfully applied for predicting the electronic absorption spectra of a number of organic compounds.[9] For example, as it has been reported for a series of sulfur-containing closed shell molecules, the PM3-CIS results can approximate those obtained from ZINDO/S and time-dependent density functional theory (TDDFT) calculations.[10] The ab initio Hartree−Fock (HF) CIS method has been used in predicting the spectroscopic properties of a number of discrete molecules, e.g., ruthenium carbide and intermetallic compounds.[11] In contrast to closed shell organic molecules, open shell transition metal complexes pose a difficult problem for the CI methods as finding a "good" CI ground state is not a straightforward process.[5] In principle, this problem can be addressed in higher-level ab initio HF methods. The high-level ab initio HF coupled-cluster with single, double, and triple substitutions (CCSD(T)),[12] multireference CI (MRCI),[13] and complete active space multiconfiguration self-consistent field (CASSCF)[14] methods, including second-order perturbation theory (CASPT2),[15] have been applied to the calculations of the vertical transition energies in small or medium-size compounds. Recently, multireference Møller−Plesset (MR-MP2)[16] and equation of motion coupled-cluster (EOM-CCSD)[17] approaches were successfully introduced for predicting the vertical excitation energy states in small organic molecules. In principle, these high-level methods can be useful, for the calculation of the vertical excitation energies of the second row transition metal complexes, although such high-level calculations are computationally demanding, and thus less attractive.

In direct methods, the excitation energies are calculated directly through the Liouville space equations.[5] The most common direct method is the random phase approximation (RPA), which not only yields accurate transition energies but also transition intensities.[5] This method can be used both with semiempirical and ab initio approaches. The density functional theory (DFT) method has been shown to offer a good alternative for computing the ground state properties of transition metal compounds.[18] Traditionally, calculations of vertical excitation energies were taken primarily as the difference between the energies of the molecular orbitals involved in the transition following Slater's "half and half" method.[4,19] Such an approach can lead to 10−50% error in the energy of transitions.[18b] The time-dependent (TD) DFT methodology provides a good compromise between the accuracy and the computational efficiency.[10,20,21] In TDDFT, the entire spectrum is calculated in a single run, and the computational costs are lower than those of the high-level ab initio methods. Also, an extended basis set is often not required. The applicability of TDDFT for calculating the properties of small open shell molecules has been described.[22] However, only a few reports on TDDFT calculations of the transition energies of molybdenum compounds have appeared.[23,24] Moreover, to our knowledge, no systematic comparison has been reported on the calculation of the vertical excitation energies for the open shell molybdenum

(5) Martin, C. H.; Zerner, M. C. In *Inorganic Electronic Structure and Spectroscopy*; Solomon, E. I., Lever, A. B. P., Eds.; Wiley & Sons Inc.: New York, 1999; pp 555−660.
(6) Ridley, J.; Zerner, M. C. *Theor. Chim. Acta* **1973**, *32*, 111−134. Zerner, M. C.; Loew, J. H.; Kirchner, E. F.; Mueller-Westerhoff, U. T.; Nazaal, A. *J. Am. Chem. Soc.* **1980**, *102*, 589−599. Neto, J. D. M.; Zerner, M. C. *Int. J. Quantum Chem.* **2001**, *81*, 187−201. Anderson, W. P.; Edwards, E. D.; Zerner, M. C. *Inorg. Chem.* **1986**, *25*, 2728−2732.
(7) Niedwieski, A. C.; Soares, J. F.; Leigh, G. J.; Nunes, F. S.; Da Motta Neto, J. D. *Int. J. Quantum Chem.* **2001**, *88*, 245−251. Estiu, G.; Cukiernik, F. D.; Maldivi, P.; Poizat, O. *Inorg. Chem.* **1999**, *38*, 3030−3039.
(8) Stewart, J. J. P. *J. Comput.-Aided Mol. Des.* **1990**, *4*, 1−105.
(9) Linnanto, J.; Korppi-Tommola, J. *J. Phys. Chem. A* **2001**, *105*, 3855−3866. Altucci, C.; Borelli, R.; de Listo, C.; De Riccardis, F.; Persico, V.; Porzio, A.; Peluso, A. *Chem. Phys. Lett.* **2002**, *354*, 160−164. Tretiak, S.; Saxena, A.; Martin, R. L.; Bishop, A. R. *Chem. Phys. Lett.* **2000**, *331*, 561−568.
(10) Fabian, J.; Diaz, L. A.; Seifert, G.; Niehaus, T. *THEOCHEM* **2002**, *594*, 41−53.
(11) Shim, I.; Kingcade, J. E.; Gingerich, K. A. *J. Chem. Phys.* **1986**, *85*, 6629−6636. Shim, I.; Finkbeiner, H. C.; Gingerich, K. A. *J. Phys. Chem.* **1987**, *91*, 3171−3178.
(12) Scuseria, G. E.; Schaefer, H. F., III. *J. Chem. Phys.* **1989**, *90*, 3700−3703. Pople, J. A.; Head-Gordon, M.; Raghavachari, K. *J. Chem. Phys.* **1987**, *87*, 5968−5975.
(13) Shepard, R.; Shavitt, I.; Pitzer, R. M.; Comeau, D. C.; Pepper, M.; Lischka, H.; Szalay, P. G.; Ahlrichs, R.; Brown, F. B.; Zhao, J.-G. *Int. J. Quantum Chem.* **1988**, *S2*, 149−165. Lischka, H.; Dallos, M.; Shepard, R. *Mol. Phys.* **2002**, *100*, 1647−1658. Chang, J.-L.; Chen, Y.-T. *J. Chem. Phys.* **2002**, *116*, 7518−7525.
(14) Roitberg, A. E.; Worthington, S. E.; Holden, M. J.; Mayhew, M. P.; Krauss, M. *J. Am. Chem. Soc.* **2000**, *122*, 7312−7316. Schlegel, H. B.; Robb, M. A. *Chem. Phys. Lett.* **1982**, *93*, 43−46.
(15) Gagliardi, L.; Orlandi, G.; Molina, V.; Malmqvist, P.-Å.; Roos, B. *J. Phys. Chem.* **2002**, *106*, 7355−7361. Schreiber, M.; Buss, V. *Phys. Chem. Chem. Phys.* **2002**, *4*, 3305−3310. Cai, Z.-L.; Reimers, J. R. *J. Phys. Chem. A* **2002**, *106*, 8769−8778.
(16) Parac, M.; Grimme, S. *J. Phys. Chem. A* **2002**, *106*, 6844−6850.
(17) Wiberg, K. B.; de Oliveira, A. E.; Trucks, G. *J. Phys. Chem. A.* **2002**, *106*, 4192−4199.
(18) (a) Parr, R. G.; Yang, W. *Density Functional Theory of Atoms and Molecules*; Oxford University Press: Oxford, 1989, 333 pp. (b) Gross, E. K. U.; Dobson, J. F.; Petersilka, M. In *Topics in Current Chemistry. Density Functional Theory II*; Nalewajski, R. F., Ed.; Springer: New York, 1996; Vol. 181, pp 81−172. (c) Schreckenbach, G.; Ziegler, T. *Theor. Chem. Acc.* **1998**, *99*, 71−82.
(19) Slater, J. C. *Adv. Quantum Chem.* **1972**, *6*, 1−92.
(20) Tozer, D.; Handy, N. C. *J. Chem. Phys.* **1998**, *109*, 10180−10189. Adamo, C.; Scuseria, G.; Barone, V. *J. Chem. Phys.* **1999**, *111*, 2889−2899. Cavillot, V.; Champagne, B. *Chem. Phys. Lett.* **2002**, *354*, 449−457. Bollinger, J. C.; Chisholm, M. H.; Click, D. R.; Folting, K.; Hadad, C. M.; Tiedtke, D. B.; Wilson, P. J. *J. Chem. Soc., Dalton Trans.* **2001**, 2074−2082.
(21) Fabian, J. *Theor. Chim. Acc.* **2001**, *106*, 199−217. Zerner, M. C.; Reidlinger, C.; Fabian, W. M. F.; Junek, H. *THEOCHEM* **2001**, *543*, 129−146. Jamorski, C.; Foresman, J. B.; Thilgen, C.; Lüthi, H.-P. *J. Chem. Phys.* **2002**, *116*, 8761−8771. Gorelsky, S. I.; Lever, A. B. P. *J. Organomet. Chem.* **2001**, *635*, 187−196. Parusel, A. B. J.; Rettig, W.; Sudholt, W. *J. Phys. Chem. A.* **2002**, *106*, 804−815. Cave, R. J.; Burke, K.; Castner, E. W., Jr. *J. Phys. Chem. A* **2002**, *106*, 9294−9305.
(22) Cai, Z.-L.; Tozer, D. J.; Reimers, J. R. *J. Chem. Phys.* **2000**, *113*, 7084−7096. Furche, F.; Ahlrichs, R. *J. Chem. Phys.* **2002**, *117*, 7433−7447.
(23) Rosa, A.; Baerends, E. J.; van Gisbergen, S. J. A.; van Lenthe, E.; Groeneveld, J. A.; Snijders, J. G. *J. Am. Chem. Soc.* **1999**, *121*, 10356−10365. Wakamatsu, K.; Nishimoto, K.; Shibahara, T. *Inorg. Chem. Commun.* **2000**, *3*, 677−679. Broclawik, E.; Borowski, T. *Chem. Phys. Lett.* **2001**, *339*, 433−437. Adamo, C.; Barone, V. *Theor. Chem. Acc.* **2000**, *105*, 169−172.
(24) Basu, P.; Nemykin, V. N.; Sengar, R. To be submitted. McNaughton, R. L.; Nemykin, V. N.; Mondal, S.; Basu, P.; Kirk, M. L. To be submitted.

systems as a function of starting geometries, basis sets, and exchange-correlation functionals.

The aim of this article is to systematically compute and compare the vertical excitation energies in a relatively simple, $[Mo^{V}OCl_4]^-$ ($S = {}^1/_2$), center calculated at different levels of theory, including TDDFT, with different basis sets, geometries, and exchange-correlation functionals. This complex was chosen because its transition energies in the UV−vis region (1−5 eV) have been precisely determined by solution and single crystal electronic and MCD spectroscopies.[25,26]

2. Computational Details

All X-ray structures for $[MoOCl_4]^-$ available in the Cambridge Crystal Structure Data Base (CSD) have been used for TDDFT calculations.[27] In addition, the geometry of the $[MoOCl_4]^-$ core was optimized at the DFT, HF, MP2, and semiempirical levels. The following methods and basis sets were used for geometry optimization: Becke's three-parameter hybrid exchange functional[28] and the gradient corrections of Perdew, along with his 1981 local correlation functional[29] (B3P86) or Lee−Yang−Parr nonlocal correlation functional[30] (B3LYP); Becke's 1988 exchange functional[33] and LYP[30] (BLYP), P86[29] (BP86), or Perdew−Wang[34] (BPW91) correlation functional, as well as HF and MP2 calculations, a DGauss full electron double-ζ basis set (DZVP) with polarization and a (18s, 12p, 9d) → [6s, 5p, 3d] contraction scheme[31] for molybdenum while the standard 6-311G(d) basis set[32] for all other atoms (designated as basis set 1). In order to understand the influence of the basis sets on optimized geometries, the following basis sets were used with the B3P86 exchange correlation functional: DZVP basis set for molybdenum and 6-311+G(d) for all other atoms (designated as basis set 2); DZVP basis set for molybdenum and 6-311++G(2d,2f) for all other atoms (designated as basis set 3); LANL2DZ effective core potential (ECP) basis set for molybdenum and 6-31G(d) for all other atoms (designated as basis set 4); LANL2DZ ECP basis set for all atoms (designated as basis set 5), and 3-21G(d) basis set for all atoms (designated as basis set 6). In all cases, frequency calculations were done in order to confirm the local minima. The following basis sets were used for TDDFT calculations: basis set 1; basis set 2; basis set 3; basis set 4; DZVP for the molybdenum atom and a 6-311+G basis set for all other atoms (designated as basis set 7); LANL2DZ ECP basis set for molybdenum and a 6-31+G(d) basis set for all other atoms (designated as basis set 8); LANL2DZ ECP for molybdenum and a 6-31+G basis set for all other atoms (designated as basis set 9); LANL2DZ ECP basis set for the molybdenum atom and a 6-31++G(2d,2f) for all other atoms (designated as basis set 10); DZVP for the molybdenum atom and a 6-311G basis set for all other atoms (designated as basis set 11); DZVP for the molybdenum atom and a 6-311G(2d) basis set for all other atoms (designated as basis set 12); LANL2DZ ECP basis set for molybdenum and a 6-31G basis set for all other atoms (designated as basis set 13); LANL2DZ ECP basis set for molybdenum and 6-31G(2d) basis set for all other atoms (designated as basis set 14). The DFT, HF, MP2, TDDFT, TD HF, and CIS HF calculations were performed on both the Windows and the Linux versions of the Gaussian 98 program.[35] Only the 16 lowest vertical excitation energies of $[MoOCl_4]^-$ were computed with TDDFT, TDHF, and CIS HF. Semiempirical calculations (ZINDO/1, ZINDO/S, and PM3(tm)) as well as extended Hückel (EH) were carried out using HyperChem software.[36] For ZINDO/S calculations, parameters for the Cl atom were implemented from the literature.[37] Two different CIS methods were used for ZINDO/1, ZINDO/S, and PM3(tm) calculations.[38a] In the first method, 10 of the highest occupied orbitals and 10 of the lowest unoccupied orbitals (10 × 10 CI) were used in single excitation configuration interactions. In the second method, all excitations with an energy less than 9 eV were considered. The 1.267 $\sigma-\sigma$ and 0.64 $\pi-\pi$ overlap weighting factors were used for all ZINDO/S calculations.[6,38a] These calculations were conducted by incorporating the recommended γ parameter set for two-electron one-center integrals and Zerner's original ionization potentials for molybdenum (referred as ZINDO/S(1)).[3a] In another set, ZINDO/S calculations were conducted by changing the ionization potential but keeping the same γ parameters (referred as ZINDO/S(2)).[3b]

3. Results and Discussions

Electronic Structures, Geometries, and Frequencies of the $[MoOCl_4]^-$ Ion.

Comparison between X-ray Crystallographically Determined and Calculated Structures of the $[MoOCl_4]^-$

(25) Carducci, M. D.; Brown, C.; Solomon, E. I.; Enemark, J. H. *J. Am. Chem. Soc.* **1994**, *116*, 11856−11868.

(26) Garner, C. D.; Hill, L. H.; Mabbs, F. E.; McFadden, D. L.; McPhail, A. T. *J. Chem. Soc., Dalton Trans.* **1977**, 1202−1207. Gray, H. B.; Hare, C. R. *Inorg. Chem.* **1962**, *1*, 363−368. Collison, D. *J. Chem. Soc., Dalton Trans.* **1990**, 2999−3006. Sabel, D. M.; Gewirth, A. A. *Inorg. Chem.* **1994**, *33*, 148−156.

(27) (a) Garner, D.; Hill, L. H.; Mabbs, F. E. *J. Chem. Soc., Dalton Trans.* **1977**, 853−858. (CSD code: PASCMO) (b) Limberg, C.; Boese, R.; Schiemenz, B. *J. Chem. Soc., Dalton Trans.* **1997**, 1633−1637. (CSD code: NABQIQ) (c) Knopp, B.; Lorcher, K.-P.; Strahle, J. *Z. Naturforsch.* **1977**, *32B*, 1361−1364. (CSD code: PASCMO1) (d) Chang, Y.-D.; Zubieta, J. *Inorg. Chim. Acta* **1996**, *245*, 177−198. (CSD code: TIXLIV) (e) Klinzing, P.; El-Kholi, A.; Muler, U.; Dehnicke, K.; Findeisen, K. *Z. Anorg. Allg. Chem.* **1989**, *569*, 83−90. (CSD code: JASRIV) (f) Blake, A. J.; Pearsons, S.; Downs, A. J.; Limberg, C. *Acta Crystallogr.* **1995**, *51C*, 571−573. (CSD code: LIMRUV)

(28) Becke, A. D. *J. Chem. Phys.* **1993**, *98*, 5648−5652.

(29) Perdew, J. P. *Phys. Rev. B* **1986**, *33*, 8822−8824.

(30) Lee, C.; Yang, W.; Parr, R. G. *Phys. Rev. B* **1988**, *37*, 785−789.

(31) Becke, A. D. *Phys. Rev. A* **1988**, *38*, 3098−3100.

(32) Perdew, J. P.; Burke, K.; Wang, Y. *Phys. Rev. B* **1996**, *54*, 16533−16539.

(33) Basis sets were obtained from the Extensible Computational Chemistry Environment Basis Set Database, Version 4/22/01, developed and distributed by the Molecular Science Computing Facility, Environmental and Molecular Sciences Laboratory, Pacific Northwest Laboratory, P.O. Box 999, WA 99352, and funded by the U.S. Department of Energy. The Pacific Northwest Laboratory is a multiprogram laboratory operated by Battelle Memorial Institute for the U.S. Department of Energy under Contract DE-AC06-76RLO 1830.

(34) McLean, A. D.; Chandler, G. S. *J. Chem. Phys.* **1980**, *72*, 5639−5948. Krishnan, R.; Binkley, J. S.; Seeger, R.; Pople, J. A. *J. Chem. Phys.* **1980**, *72*, 650−654.

(35) Frisch, M. J.; Trucks, G. W.; Schlegel, H. B.; Scuseria, G. E.; Robb, M. A.; Cheeseman, J. R.; Zakrzewski, V. G.; Montgomery, J. A., Jr.; Stratmann, R. E.; Burant, J. C.; Dapprich, S.; Millam, J. M.; Daniels, A. D.; Kudin, K. N.; Strain, M. C.; Farkas, O.; Tomasi, J.; Barone, V.; Cossi, M.; Cammi, R.; Mennucci, B.; Pomelli, C.; Adamo, C.; Clifford, S.; Ochterski, J.; Petersson, G. A.; Ayala, P. Y.; Cui, Q.; Morokuma, K.; Malick, D. K.; Rabuck, A. D.; Raghavachari, K.; Foresman, J. B.; Cioslowski, J.; Ortiz, J. V.; Stefanov, B. B.; Liu, G.; Liashenko, A.; Piskorz, P.; Komaromi, I.; Gomperts, R.; Martin, R. L.; Fox, D. J.; Keith, T.; Al-Laham, M. A.; Peng, C. Y.; Nanayakkara, A.; Gonzalez, C.; Challacombe, M.; Gill, P. M. W.; Johnson, B. G.; Chen, W.; Wong, M. W.; Andres, J. L.; Head-Gordon, M.; Replogle, E. S.; Pople, J. A. *Gaussian 98*; Gaussian, Inc.: Pittsburgh, PA, 1998.

(36) *HyperChem Pro. 6.03*; HyperCube, Inc.: Gainesville, FL, 2001.

(37) Gorelsky, S. I.; Kotov, V. Yu. *Russ. J. Coord. Chem.* **1998**, *24*, 491−494. Renouard, T.; Fallahpour, R.-A.; Nazeeruddin, M. K.; Humphrey-Baker, R.; Gorelsky, S. I.; Lever, A. B. P.; Grätzel, M. *Inorg. Chem.* **2002**, *41*, 367−378.

(38) (a) *HyperChem Reference Manual*; HyperCube, Inc.: Gainesville, FL, 1996; 637 pp. (b) Parr, R. G. *The Quantum Chemistry of Molecular Electronic Structure*; W. A. Benjamin Inc.: New York, 1964; p 510.

Table 1. X-ray Determined and Optimized Parameters for the $[MoOCl_4]^-$ Core

CSD code or method used	Mo═O, Å	Mo—Cl, Å	O—Mo—Cl, deg
TIXLIV	1.589	2.328	104.84
PASCMO	1.609	2.333	105.26
JAJRIV	1.640	2.355	100.94
LIMRUV	1.646	2.342	105.24
NABQIQ	1.668	2.354	101.53
PASCMO1	1.717	2.337	104.52
av	1.645	2.342	103.72
B3P86 DZVP/6-311G(d)	1.690	2.375	105.29
B3P86 DZVP/6-311+G(d)	1.688	2.375	105.60
B3P86 DZVP/6-311++G(2d,2f)	1.682	2.369	105.75
B3LYP DZVP/6-311G(d)	1.699	2.400	105.27
BLYP DZVP/6-311G(d)	1.726	2.424	105.24
BP86 DZVP/6-311G(d)	1.716	2.397	105.26
HF/MP2 DZVP/6-311G(d)	1.733	2.466	108.33
HF DZVP/6-311G(d)	1.645	2.463	110.20
PM3	1.648	2.372	108.58
ZINDO/1	1.712	2.396	106.13
B3P86 LANL2DZ/6-31G(d)	1.689	2.408	105.22
B3P86 LANL2DZ	1.671	2.374	105.49
B3P86 3-21G(d)	1.689	2.375	104.62

Ion. The X-ray crystallographically determined bond distances and angles for the $[MoOCl_4]^-$ ion are presented in Table 1. While the experimental Mo—Cl distances are nearly constant (the largest deviation is 0.027 Å), the deviations of the Mo═O bond distance and O—Mo—Cl angles are ±0.128 Å and ±4.314°, respectively. We also have probed the structure of $[MoOCl_4]^-$ through geometry optimization at the semiempirical, HF, and DFT levels (Table 1). There are no well-defined criteria for comparing the "goodness" of computed geometries at different levels of theory and experimental data. For example, the accepted geometry obtained from a molecular mechanics calculation deviate significantly from the experimental values,[39] while a more stringent condition is applied for ab initio and DFT methods (typically 0.03 Å for the bond distances and less than 1° for the angles).[40] To evaluate the accuracy of the calculated geometry, we have used the upper and the lower limits of the crystallographically determined bond distances within ±0.03 Å and angles within ±0.5° error reflecting the variance in the experimental data. In the semiempirical calculations, the Mo═O distances lie within the experimentally observed values. However, the Mo—Cl distance is overestimated in ZINDO/1 formalism, and the O—Mo—Cl angle is overestimated in the PM3 method. Both HF and MP2 algorithms (basis set 1) overestimate the Mo—Cl distance as well as the O—Mo—Cl angle. Pure DFT and B3LYP approaches (basis set 1) overestimate the Mo—Cl bond distance, while Mo═O and O—Mo—Cl parameters are in reasonable agreement with the experimental data. Finally, the geometry calculated with the B3P86 exchange correlation functional (basis set 1) for the $[MoOCl_4]^-$ ion is in accord with the experimental data. This is in agreement with the suggestion that, in comparison to pure DFT and hybrid B3LYP approaches, the B3P86 EC functional gives more accurate geometry, although the difference is small.[41]

To explore the influence of different basis sets on the calculated geometries, B3P86 optimizations with basis sets 2−6 were conducted. The addition of diffuse and polarization functions to basis set 1 slightly decreases both the Mo═O and the Mo—Cl distances with a concomitant increase in the O—Mo—Cl angle. Interestingly, the geometry obtained from the smallest basis set, basis set 6, is also in good agreement with the experimental data. The calculations using the ECP LANL2DZ basis sets (basis sets 4 and 5) provide a good agreement with the experimental data with the exception of the Mo—Cl distance that was overestimated when basis set 4 was used. In summary, the optimized geometries for the $[MoOCl_4]^-$ complex are within ±0.03 Å and ±0.5°, for distances and angles respectively, of the experimental values only when they were optimized using a DFT approach coupled with the B3P86 exchange-correlation functional and basis sets 1−3, 5, and 6.

Comparison of the Calculated Vibrational Frequencies of the $[MoOCl_4]^-$ Ion. From the nine normal modes of vibration of the tetragonally distorted square pyramidal $[MoOCl_4]^-$ ion, only the A_1 and E vibrations are infrared active, while nine vibrations of A_1 (three), B_1 (two), B_2 (one), and E (three) symmetries are Raman active (Figure S1).[42] Table 2 lists the calculated and experimental vibrational frequencies of the $[MoOCl_4]^-$ core. The semiempirical calculations do not agree with the experimental data, while the DFT methods are in reasonable agreement with the experiment (Table 2). Because the HF and MP2 methods resulted in a $^2A_2$ electronic ground state that is different from the experimentally observed $^2B_2$ state, no further discussion on the results from these methods is made. Calculations with basis set 1 and the pure DFT EC functionals (BLYP and BP86) are in poor agreement with the experimental data, while those with hybrid EC functionals show better agreement. It is interesting to note that the calculated A_1, B_2, and E frequencies were in accord with the experimental data, while the energies of the B_1 frequencies were underestimated. Again, in comparison to the B3LYP results, the frequencies calculated using the B3P86 EC functional are in slightly closer agreement with the experiment. The average deviation for A_1, B_2, and E vibrations was ∼15 cm^{-1}, in the case of the B3P86 EC functional, while it was ∼21 cm^{-1} in case of B3LYP. Moreover, the three low energy vibrations ($1A_1$, 1E, and $2A_1$), calculated by the B3P86 EC functional, were in excellent agreement with the experimental data, while the agreement with the B3LYP calculations was poor. Finally, the data presented in Table 2 clearly suggests that the implementation of diffuse and additional polarization functions into the basis set did not improve the results significantly.

Comparison of the Calculated Electronic Structure of the $[MoOCl_4]^-$ Ion. A typical example of the calculated orbital energies and compositions of the $[MoOCl_4]^-$ core, using unrestricted DFT formalism, is presented in Table 3,

(39) Rappe, A. K.; Goddard, W. A., III. *J. Phys. Chem.* **1991**, *95*, 3358−3363. Rappe, A. K.; Casewit, C. J.; Colwell, K. S.; Goddard, W. A., III; Skiff, W. M. *J. Am. Chem. Soc.* **1992**, *114*, 10024−10035.

(40) Guillemoles, J.-F.; Barone, V.; Joubert, L.; Adamo, C. *J. Phys. Chem. A* **2002**, *106*, 11354−11360.

(41) Zarić, S.; Hall, M. B. In *Molecular Modelling and Dynamics of Bioinorganic Systems*; Banci, L., Comba, P., Eds.; Kluwer Academic Publishers: Norwell, MA, 1997; pp 255−277. Thomson, L. M.; Hall, M. B. *J. Am. Chem. Soc.* **2001**, *123*, 3995−4002.

(42) Collin, R. G.; Griffith, W. P.; Pawson, D. *J. Mol. Struct.* **1973**, *19*, 531−544.

Table 2. Experimental and Calculated Frequencies (in cm^{-1}) for the $[MoOCl_4]^-$ Core

method//basis set	ν_1 (A_1)	ν_2 (A_1)	ν_3 (A_1)	ν_4 (B_1)	ν_5 (B_1)	ν_6 (B_2)	ν_7 (E)	ν_8 (E)	ν_9 (E)	MAD	mean dev
B3P86//1	1006	347	152	271	41	187	364	237	155	31	17
B3P86//2	1008	347	152	271	42	186	365	233	154	31	18
B3P86//3	1026	350	152	275	43	181	369	235	151	31	15
B3P86//4	1031	331	146	263	44	174	362	232	148	35	20
B3P86//5	1054	336	152	253	42	184	350	236	154	40	17
B3P86//6	1063	338	147	271	51	174	372	240	146	35	13
B3LYP//1	991	335	150	260	38	183	351	230	152	38	25
BP86//1	948	329	147	257	38	180	347	225	149	44	33
BLYP//1	930	316	144	246	35	176	333	221	146	50	41
PM3	1187	428	136	340	45	130	465	195	115	68	14
ZINDO/1	1228	467	159	388	50	175	519	244	150	81	52
exptl[42]	1008	354	184	327	158	167	364	240	114		

Table 3. Calculated Molecular Orbital Energies and Compositions of the $[MoOCl_4]^-$ Core with the Geometry Obtained from the Structure with CSD Code JAJRIV Using B3P86 EC Functional[a]

		α set composition, %					*β* set composition, %			
orbital	*E*, eV	Mo	Mo(d)	O	Cl	*E*, eV	Mo	Mo(d)	O	Cl
					Basis Set 1					
13e	−5.388	0.6	0.0	8.2	91.2	−5.397	0.7	0.1	8.1	91.3
$8b_1$	−5.191	0.0	0.0	0.0	100.0	−5.179	0.0	0.0	0.0	100.0
14e	−5.183	1.8	0.7	1.3	96.8	−5.030	1.4	0.5	0.8	97.8
$2a_2$	−4.608	0.0	0.0	0.0	100.0	−4.429	0.0	0.0	0.0	100.0
$4b_1$	−3.644	70.4	70.4	0.0	29.6	−0.691	83.5	83.5	0.0	16.5
15e	−0.159	73.4	72.3	15.1	11.5	0.140	75.4	74.3	13.6	11.0
$9b_2$	1.207	59.0	59.0	0.0	41.0	1.413	59.9	59.9	0.0	40.1
$19a_1$	1.654	75.0	40.1	14.2	10.9	1.855	76.6	38.8	13.1	10.4
					Basis Set 4					
10e	−5.180	1.0	0.5	9.2	89.8	−5.183	1.0	0.5	9.1	89.9
$7b_1$	−4.978	0.5	0.5	0.0	99.5	−4.965	0.6	0.6	0.0	99.4
11e	−4.953	1.1	0.4	1.6	97.3	−4.796	1.0	0.3	0.9	98.1
$2a_2$	−4.379	0.0	0.0	0.0	100.0	−4.193	0.0	0.0	0.0	100.0
$3b_1$	−3.426	60.2	60.2	0.0	39.8	−0.407	72.9	72.9	0.0	27.1
12e	0.167	60.9	57.3	19.6	19.5	0.476	62.4	58.6	18.2	19.5
$8b_2$	1.510	46.7	46.7	0.0	53.3	1.709	47.0	47.0	0.0	53.0
$13a_1$	1.960	62.7	39.3	25.5	11.7	2.169	65.2	37.9	24.1	10.6

[a] As an example.

while the complete list is presented in Table S1 and that for semiempirical methods is in Table S2. The pictorial representations of selected orbitals are presented in Figures 1 and 2. The ligand field theory (LFT),[43] along with EPR, UV−vis, and MCD spectral data for $[MoOCl_4]^-$ (including single crystal polarized spectra collected at a low-temperature), suggests that the d-orbitals in the $[MoOCl_4]^-$ complex follow the order $4d_{xy} < 4d_{xz,yz} < 4d_{x^2-y^2} < 4d_{z^2} < 5s$, similar to other pentacoordinated mono-oxo molybdenum compounds.[25,26]

The DFT calculations show that the semioccupied molecular orbital is primarily composed of the Mo $4d_{xy}$ orbital agreeing well with the UV−vis, MCD, and EPR data.[25,26] This orbital consists of 70−72% $4d_{xy}$ character (depending on the geometry) and 30−28% chlorine atom character for the α orbital set (basis set 1), while the metal contribution is smaller and the contribution from the chlorine atoms is larger for basis set 4 (60−62% and 40−38%, respectively). A similar basis set dependency is observed for the *β* orbitals despite a larger metal contribution presumably due to the spin polarization.[44] This is not uncommon in systems with a significant metal−ligand character and results primarily from a small energy difference between the metal and the ligand orbitals.[44] A similar situation has also been observed in

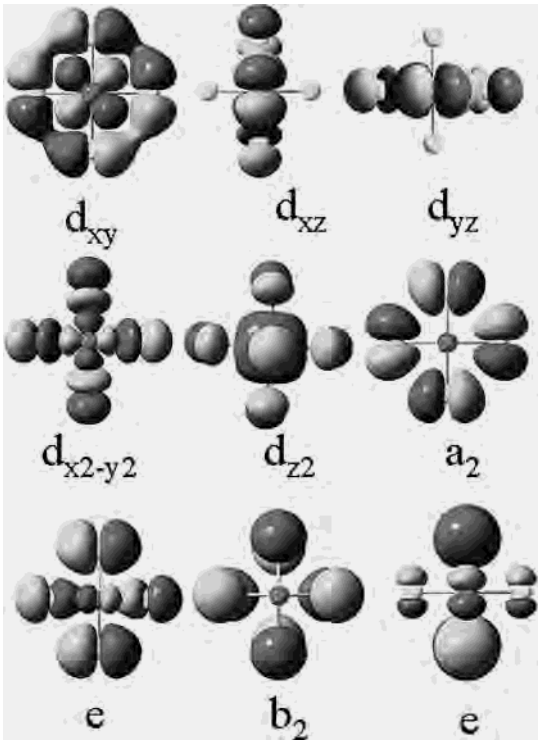

Figure 1. Typical shapes of the molybdenum manifold and selected ligand based molecular orbitals in the $[MoOCl_4]^-$ core calculated at B3P86 DFT level.

$[MoO(SR)_4]^-$ complexes, which leads to an increase in the d−d transition intensity.[24] The calculated LUMO orbitals consist of the d_{xz} and the d_{yz} orbitals and show considerable Mo═O antibonding character (Figure 2). The effective displacement of the molybdenum atom out of the *xy* plane (i.e., away from the Mo−Cl bond vectors) reduces the interaction between the molybdenum $d_{x^2-y^2}$ orbital and pseudo-Cl^{σ} orbitals resulting in a reduction in the energy of this orbital.

In all cases, the ligand field (LF) is dominated by the terminal oxo ligand, and the energy of the d_{z^2} orbital is dependent on the Mo═O bond length: the shorter this bond, the higher the energy of the d_{z^2} orbital. The difference in energy between the d_{z^2} and $d_{x^2-y^2}$ orbitals depends on the Mo═O distance; however, the O−Mo−Cl angle also has a

(43) Figgis, B. N. *Introduction to Ligand Fields*; John Wiley & Sons: New York, 1966; p 351.

(44) Noodleman, J. L. L.; Case, D. A. In *Inorganic Electronic Structure and Spectroscopy*; Solomon, E. I., Lever, A. B. P., Eds.; Wiley & Sons Inc.: New York, 1999; pp 661−724. Noodelman, L.; Peng, C. Y.; Case, D. A.; Mouesca, J.-M. *Coord. Chem. Rev.* **1995**, *144*, 199−244.

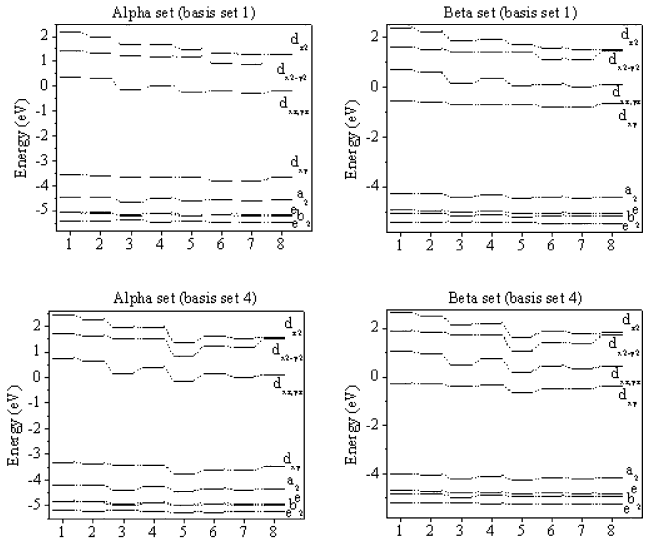

Figure 2. The orbital diagram for the $[MoOCl_4]^-$ complex calculated at the B3P86 DFT level using unrestricted-open formalism with basis sets 1 and 4. The following starting geometries were used: 1, TIXLIV; 2, PASCMO; 3, JAJRIV; 4, LIMRUU; 5, NABQIQ; 6, optimized at B3P86 basis set 3; 7, optimized at B3P86 basis set 6; 8, PASCMO1.

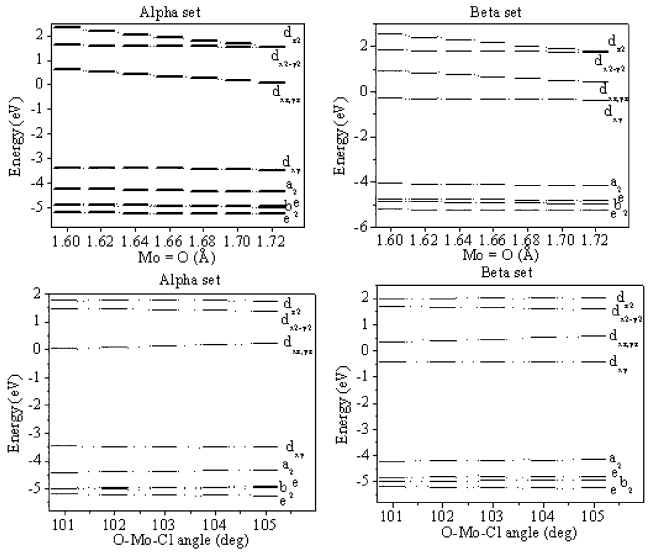

Figure 3. Molecular orbital energies as a function of Mo═O distance and O—Mo—Cl angle obtained from the B3P86 EC calculations with basis set 4.

similar influence. When a crystallographically determined geometry (CSD code PASCMO)[27a] was used (Mo═O distance, 1.61 Å; O—Mo—Cl angle, 105.26°), the energy difference between these orbitals is 0.77 eV (d_{z^2} orbital is higher in energy). For another structure (CSD code PASCMO1), the Mo═O distance was found to be 1.72 Å, the O—Mo—Cl angle was 104.52°,[27c] and the orbitals were almost degenerate (energy differences 0.03 and 0.11 eV for α and β sets, respectively, with basis set 1). However, from these calculations it is difficult to assert whether the Mo═O distance or the O—Mo—Cl angle plays a dominant role in dictating the order of the orbitals because X-ray structures show changes in both parameters simultaneously. To clarify this ambiguity, two different sets of calculations were done. In the first case, the Mo═O distance was reduced from 1.72 to 1.60 Å with 0.2 Å steps, while all other parameters were kept constant (Mo—Cl distance 2.337 Å; O—Mo—Cl angle 104.52°). In the second set, O—Mo—Cl angle was changed from 101° to 105° by 1° increments, while the Mo═O and the Mo—Cl distances were kept constant at 1.668 and 2.337 Å, respectively. The results of these two sets of calculations are presented in Table S3 and Figure 3. An increase in the Mo═O distance should lead to a stabilization of the d_{z^2} orbital and decrease the energy difference between the d_{z^2} and $d_{x^2-y^2}$ orbitals, with the energy of the $d_{x^2-y^2}$ orbital remaining nearly invariant. Indeed, the energy difference between the d_{z^2} and $d_{x^2-y^2}$ orbitals increases from 0.02 to 0.69 eV when the Mo═O bond distance is reduced from 1.72 to 1.60 Å. In such cases, all of the out-of-plane molybdenum orbitals (d_{z^2} and d_{xz}, d_{yz}) are also stabilized by 0.77 and 0.53 eV, respectively, while the in-plane, d_{xy} and $d_{x^2-y^2}$, orbitals are stabilized only by 0.1 eV. On the other hand, an increase in the O—Mo—Cl angle leads to a stabilization of the $d_{x^2-y^2}$ and d_{xy} orbitals while the energy of the d_{z^2} orbital remains nearly constant. As a result, the energy difference between the d_{z^2} and $d_{x^2-y^2}$ orbitals increases. Also, an increase of the O—Mo—Cl angle leads to an increase in antibonding interactions between chlorine out-of-plane orbitals and the molybdenum d_{xz} and d_{yz} orbitals making them less stable by 0.2 eV.

Finally, the six highest energy fully occupied orbitals are practically pure chlorine in- and out-of-plane orbitals. They follow the $a_2 > e \approx b_1 > e$ order where the first e and b_1 orbitals are practically degenerate for the α set orbitals. In addition, the in-plane orbitals of Cl are higher in energy than the out-of-plane orbitals, and a similar picture was derived from Xα calculations.[45] Semiempirical ZINDO/S(2) and EH calculations give a similar order for the occupied orbitals, while the ZINDO/S(1) and the PM3 methods raise the 5e orbital higher than the $1a_2$ orbital (Table S2). Finally, the ZINDO/1 method gives the orbital order as $3b_1 < 4e < 1a_2 < 5e$. All semiempirical and EH calculations yield a HOMO orbital that is predominantly Mo d_{xy} in character, although the ordering of the Mo d-orbitals is different from those predicted from the LFT or the experimental data. Thus, in the case of the PM3(tm) calculations, the LUMO is the molybdenum 5s orbital, found to be between the d-orbitals following the order $4d_{xy} < 5s < 4d_{xz,yz} < 4d_{x^2-y^2} < 4d_{z^2}$. In the case of ZINDO/1 and ZINDO/S(1) calculations, the LUMO and LUMO + 1 are always the molybdenum 5s and $4d_{z^2}$ orbitals, respectively (Table S2), and are also not in the expected order, while in the case of ZINDO/S(2) the orbital order is $4d_{xy} < 4d_{xz,yz} < 5s < 4d_{z^2} < 4d_{x^2-y^2}$. Finally, in the EH calculations the molybdenum $4d_{z^2}$ orbital was found to be the LUMO. Taken together, it can be concluded that the order of the orbitals for the molybdenum metal manifold can be predicted correctly only from high-level DFT calculations, while semiempirical and EH calculations provide a poor picture.

Calculation of the Vertical Excitation Energies of $[MoOCl_4]^-$ Ion. In evaluating the performance of any

(45) Deeth, R. J. *J. Chem. Soc., Dalton Trans.* **1991**, 1895−1900. Weber, J.; Garner, C. D. *Inorg. Chem.* **1980**, *19*, 2206−2209. Sunil, K. K.; Harrison, J. F.; Rogers, M. T. *J. Chem. Phys.* **1982**, *76*, 3087−3097.

method for calculating the vertical excitation energies, three factors should be considered. First, the vertical excitation energies are not observable experimentally, even at a very low-temperature, and a comparison of the calculated vertical excitation energies with experiments is approximate.[46] Second, the solution spectra (liquid or frozen) are often affected by polar and protic solvents; similarly, in the solid state, the crystal lattice forces can affect the band positions. Thus, the calculated gas-phase spectrum can be different from those spectra recorded in solution or in single crystal experiments.[40,47] Finally, the asymmetry in any absorption band can be taken as a result of several overlapping bands. For example, the broad band around 2 eV for $[MoO(SPh)_4]^-$ consists of at least four overlapped bands.[48] In these cases, it is difficult to precisely define the individual band positions. Fortunately, in the case of the $[MoOCl_4]^-$ ion the lowest energy d−d transitions are distinctly separate from the other bands and can be used as a marker for the comparison. Moreover, from the MCD studies the intense CT band at ∼30000 cm^{-1} has been interpreted as a composite of only two overlapping pseudo-A-term bands providing a mode for separation.[25,26]

The reported[25] band assignment of $[MoOCl_4]^-$ is used for the discussion of the calculated vertical excitation energies of bands 1−6, while bands 7−9 are introduced in a following paragraph. The simplest and fastest way to calculate vertical excitation energies for the $[MoOCl_4]^-$ complex is the well-known EH method. In this case, transition energies can be calculated as a simple energy difference between the orbitals of interest.[38b] The EH method underestimates all of the vertical excitation energies for LF transitions (Table S4). The LF transitions for the $[MoOCl_4]^-$ and the $[MoOCl_4(H_2O)]^-$ complexes were observed at ca. 1.98 eV ($d_{xy} \rightarrow d_{xz,yz}$) and 2.96 eV ($d_{xy} \rightarrow d_{x^2-y^2}$),[25,26] while the calculated values were 0.56 and 2.83 eV, respectively. Moreover, the EH theory incorrectly predicts the $d_{xy} \rightarrow d_{z^2}$ transition at 0.80 eV, while the CT transitions (bands 3−6, vide infra) are overestimated by 0.33−0.68 eV. Because the orbital order calculated by the EH approach, especially the molybdenum metal-fold, is in poor agreement with the experimental data, higher-level calculations, and LFT, it can be concluded that the EH method does not provide a realistic picture.

Among the semiempirical calculations, ZINDO methods are popular in predicting the transition energies for inorganic compounds.[5−7] The parameters for molybdenum in the ZINDO/1 method were published about 10 years ago.[49] In the original paper, the authors noted that, even for the ZINDO/1 level with $\sigma-\sigma$ and $\pi-\pi$ overlap weighting factors equal to 1, the transition energies for simple second row transition metal hydrides can be accurately predicted.[49] However, the lowest transition energy, i.e., the d−d transition for $[MoOCl_4]^-$ calculated by the ZINDO/1 to be 2.45 eV (observed 1.98 eV), and the other transitions, especially the CT band transitions, are also overestimated (Table S4). The results are not surprising as, in the ZINDO/1 approach, the two-electron integrals compute analytically, while in the ZINDO/S model they are empirically set to match atomic spectroscopy.[5,6,49] This is the primary reason, in most cases, for the greater success of the ZINDO/S method in representing the UV−vis spectra.[5] The lowest energy d−d transition calculated by the ZINDO/S(1) method differs from the experimental results by 0.50 eV while the overestimation of the CT bands is even more significant (Table S4). The first d−d transition calculated at the ZINDO/S(2) level is in reasonable agreement with the experimental data, while other energies are overestimated by 0.52−3.38 eV (Table S4). Interestingly, the ZINDO/S method is often accurate for computing $\pi-\pi^*$ and $n-\pi^*$ type transitions, although the LMCT or MLCT energies are often overestimated.[3,50] Surprisingly, all d−d transitions calculated, at the PM3(tm) level, agree well with the experimental data (Table S4); however, the CT energies are underestimated by 0.78−1.27 eV. Taken together, the vertical excitation energies calculated by the semiempirical methods tested here do not agree with the experimental data.

The high-level correlated ab initio calculations such as CASSCF,[14] MRCI,[13] CCSD(T),[12] and MCCSF[51] are computationally expensive, while the comparatively inexpensive ab initio methods with CIS algorithm gave the lowest energy transition with meaningless energy. The TDHF calculations did not show any significant improvement over CIS HF calculations. The unrealistic transition energy description may be a result of the convergence of the HF function to a $^2A_2$ ground state. In contrast to the methods described already, the TDDFT calculations resulted in transition energies that are in reasonable agreement with the experimental data. Results from the B3P86 exchange-correlation functional calculations on the X-ray derived and optimized geometries with basis sets 1 and 4 are listed in Tables 4 and 5. Here, the mean deviation lies between −0.01 and 0.33 eV, and the median average deviation (MAD) lies between 0.13 and 0.33 eV. Such a dramatic improvement, of TDDFT over CIS HF or TDHF calculations, can be attributed to two reasons. First, both the exchange and correlation effects are included in the EC functional, resulting in better quality DFT orbitals.[20,21] Second, in continuum DFT theory, the potential varies smoothly as a function of the number of electrons leading to orbital independence in the functional; all orbitals are eigenfunctions of the same Kohn−Sham operator, involving ($N - 1$) electron potentials.[52] In contrast, TDHF orbitals consist of eigenfunctions of an N electron potential.

(46) Lever, A. B. P. *Inorganic Electronic Spectroscopy*, 2nd ed.; Elsevier Science Publishing: New York, 1986; 864 pp.
(47) Foresman, J. B.; Frisch, A. *Exploring Chemistry with Electronic Structure Methods*; Gaussian, Inc.: Pittsburgh, PA, 1996; p 302.
(48) McNaughton, R. L.; Tipton, A. A.; Rubie, N. D.; Conry, R. R.; Kirk, M. L. *Inorg. Chem.* **2000**, *39*, 5697−5706. McMaster, J.; Carducci, M. D.; Yang, Y.-S.; Solomon, E. I.; Enemark, J. H. *Inorg. Chem.* **2001**, *40*, 687−702.
(49) Anderson, W. P.; Cundari, T. R., Zerner, M. C. *Int. J. Quantum Chem.* **1991**, *39*, 31−45.
(50) Thompson, M. A.; Zerner, M. C. *J. Am. Chem. Soc.* **1991**, *113*, 8210−8215. Du, P.; Axe, F. U.; Loew, G. H.; Canuto, S.; Zerner, M. C. *J. Am. Chem. Soc.* **1991**, *113*, 8614−8621.
(51) Yamamoto, N.; Vreven, T.; Robb, M. A.; Frisch, M. J.; Schlegel, H. B. *Chem. Phys. Lett.* **1996**, *250*, 373−378.
(52) Tozer, D. J.; Handy, N. C. *Phys. Chem. Chem. Phys.* **2000**, *2*, 2117−2121.

Table 4. Vertical Excitation Energies of the [MoOCl$_4$]$^-$ Core from Crystallography and Optimized Geometries Calculated by the TDDFT Approach Coupled with a uB3P86 Exchange-Correlation Functional and Basis Set 1

transition		calcd energy, eV ($f \times 10^2$), for each geometry used								
composition[a]	excited state	TIXLIV	PASCMO	JAJRIV	LIMRUV	NABQIQ	PASCMO1	opt1[b]	opt2[c]	exptl[d]
$d_{xy} \rightarrow d_{xz,yz}$	^2E	2.09 (0)	2.04 (0)	1.66 (0)	1.90 (0)	1.61 (0.01)	1.65 (0)	1.80 (0)	1.72 (0)	1.98
$d_{xy} \rightarrow d_{x^2-y^2}$	$^2B_1$	3.00 (0)	2.97 (0)	2.93 (0)	2.92 (0)	2.92 (0)	2.96 (0)	2.79 (0)	2.78 (0)	2.96
$d_{xy} \rightarrow d_{z^2}$	$^2A_1$	4.07 (0)	3.93 (0)	3.67 (0)	3.68 (0)	3.50 (0)	3.26 (0)	3.44 (0)	3.39 (0)	4.26
$2a_2 \rightarrow d_{xy}$	$^2A_2$	2.65 (0)	2.64 (0)	2.70 (0)	2.64 (0)	2.71 (0)	2.70 (0)	2.58 (0)	2.60 (0)	
$14e \rightarrow d_{xy}$	^2E	3.28 (2.89)	3.27 (2.73)	3.25 (2.39)	3.25 (2.48)	3.25 (1.47)	3.32 (1.73)	3.16 (2.10)	3.16 (1.92)	3.50
$8b_1 \rightarrow d_{xy}$	$^2B_1$	3.31 (0)	3.29 (0)	3.32 (0)	3.28 (0)	3.32 (0)	3.35 (0)	3.19 (0)	3.20 (0)	3.25
$13e \rightarrow d_{xy}$	^2E	3.63 (0.15)	3.61 (0.19)	3.51(0.01)	3.59 (0.12)	3.52 (0.03)	3.60 (0.1)	3.50 (0.11)	3.47 (0.09)	3.78
$2a_2^e \rightarrow d_{xz,yz}$	^2E	3.73 (0.02)	3.65 (0)	3.36 (0.3)	3.49 (0.1)	3.30 (1.02)	3.26 (0.46)	3.31 (0.14)	3.25 (0.29)	
$2a_2^f \rightarrow d_{xz,yz}$	^2E	3.86 (0.04)	3.78 (0.03)	3.48 (0.05)	3.63 (0.03)	3.42 (0.04)	3.43 (0.02)	3.45 (0.04)	3.39 (0.03)	
mean dev		0.06	0.10	0.23	0.18	0.27	0.26	0.31	0.33	
MAD		0.13	0.14	0.25	0.19	0.29	0.30	0.31	0.33	

[a] Predominant contribution: d_{xy} has a $4b_2$ index, $d_{xz,yz}$ have a 15e index, $d_{x^2-y^2}$ has a $9b_1$ index, d_{z^2} has a $19a_1$ index. [b] Optimized with the uB3P86 exchange-correlation functional and basis set 3 level geometry. [c] Optimized with the uB3P86 exchange-correlation functional and basis set 6 geometry. [d] References 25 and 26. [e] α set. [f] β set.

Table 5. Vertical Excitation Energies of the [MoOCl$_4$]$^-$ Core from Crystallography and Some Optimized Geometries, Calculated by Using the TDDFT Approach Coupled with a uB3P86 Exchange-Correlation Functional and Basis Set 4

transition		calcd energy, eV ($f \times 10^2$), for each geometry used								
composition[a]	excited state	TIXLIV	PASCMO	JAJRIV	LIMRUV	NABQIQ	PASCMO1	opt1[b]	opt2[c]	exptl[d]
$d_{xy} \rightarrow d_{xz,yz}$	^2E	2.18 (0)	2.12 (0)	1.74 (0)	1.98 (0)	1.68 (0)	1.71 (0)	1.88 (0)	1.78 (0)	1.98
$d_{xy} \rightarrow d_{x^2-y^2}$	$^2B_1$	3.03 (0)	3.00 (0)	2.96 (0)	2.95 (0)	2.95 (0)	2.99 (0)	2.81 (0)	2.80 (0)	2.96
$d_{xy} \rightarrow d_{z^2}$	$^2A_1$	4.08 (0)	3.94 (0)	3.73 (0)	3.72 (0)	3.57 (0)	3.33 (0)	3.50 (0)	3.46 (0)	4.26
$2a_2 \rightarrow d_{xy}$	$^2A_2$	2.73 (0)	2.72 (0)	2.77 (0)	2.75 (0)	2.77 (0)	2.75 (0)	2.64 (0)	2.66 (0)	
$11e \rightarrow d_{xy}$	^2E	3.36 (2.74)	3.34 (2.58)	3.32 (2.29)	3.38 (1.49)	3.31 (1.56)	3.38 (1.49)	3.22 (1.96)	3.22 (1.79)	3.50
$7b_1 \rightarrow d_{xy}$	$^2B_1$	3.40 (0)	3.37 (0)	3.39 (0)	3.41 (0)	3.39 (0)	3.41 (0)	3.26 (0)	3.27 (0)	3.25
$10e \rightarrow d_{xy}$	^2E	3.73 (0.16)	3.71 (0.19)	3.59 (0)	3.68 (0.12)	3.59 (0.03)	3.67 (0.1)	3.58 (0.1)	3.55 (0.08)	3.78
$2a_2^e \rightarrow d_{xz,yz}$	^2E	3.84 (0.04)	3.75 (0.01)	3.44 (0.29)	3.58 (0.12)	3.38 (0.83)	3.32 (0.6)	3.38 (0.16)	3.32 (0.32)	
$2a_2^f \rightarrow d_{xz,yz}$	^2E	3.98 (0.06)	3.90 (0.05)	3.58 (0.07)	3.73 (0.04)	3.50 (0.05)	3.50 (0.04)	3.54 (0.06)	3.47 (0.04)	
mean dev		−0.01	0.04	0.17	0.12	0.21	0.21	0.25	0.27	
MAD		0.13	0.14	0.21	0.16	0.25	0.27	0.25	0.28	

[a] Predominant contribution: d_{xy} has a $3b_2$ index, $d_{xz,yz}$ have a 12e index, $d_{x^2-y^2}$ has a $8b_1$ index, d_{z^2} has a $13a_1$ index. [b] Optimized at a uB3P86 exchange-correlation functional with basis set 3 level geometry. [c] Optimized at a uB3P86 exchange-correlation functional with basis set 6 geometry. [d] References 25 and 26. [e] α set. [f] β set.

Before discussing the influence of the basis sets and geometries on the calculated transition energies, the computed vertical excitation energies are compared with the spectroscopic assignments described in the literature; analogies are also drawn to theoretical reports[45,53] (Table S5). In addition, the possible low-energy transitions of the [MoOCl$_4$]$^-$ ion are presented in Figure S2.

Band 1. The first band is calculated to a $d_{xy} \rightarrow d_{xz}$,$d_{yz}$ ($^2E \leftarrow {}^2B_2$) ligand field transition with *x*,*y* polarization in the C_{4v} point group, which is in agreement with the experimental assignment. In all cases, this band has the lowest vertical excitation energy independent of the exchange-correlation functionals, geometries, and basis sets. While the transition energy calculated for this band shows significant dependence on the geometry and the basis set used, the band intensity has always been computed to be zero, which is expected for a symmetry allowed d−d transition.

Band 2. The third calculated transition has been observed optically but was assigned to be the second band. Following the experimental notation, here we refer to this band as band 2, although it represents the third calculated band. This is an allowed $d_{xy} \rightarrow d_{x^2-y^2}$ ($^2B_1 \leftarrow {}^2B_2$) ligand field transition with *z* polarization. Unlike band 1, this transition does not vary significantly in energy as a function of the geometry and the basis set used. However, the intensity remained zero.

Band 3. The second transition was calculated to be an $a_2 \rightarrow d_{xy}$ ($^2A_2 \leftarrow {}^2B_2$) charge transfer transition from the chlorine 3p in-plane orbitals to the molybdenum $4d_{xy}$ orbital. This transition is symmetry forbidden in the C_{4v} group and has not been observed in [MoOX$_4$]$^-$ (X = halogen) complexes. However, this transition has been observed in the case of the [MoOCl$_4$(H$_2$O)]$^-$ complex at ca. 3.00 eV (mentioned as band 3 in ref 25), probably because of the reduction in symmetry (from C_{4v} to C_{2v}) or vibronic coupling. Because the position of this band has not been supported experimentally, the calculated band position was not used for the mean deviation and MAD analysis. This band is referred to as band 3, although it is the second calculated band.

Band 4. The fourth experimentally observed band is due to a $b_1 \rightarrow d_{xy}$ ($^2B_2 \leftarrow {}^2B_1$) charge transfer transition that is orbitally forbidden but can gain intensity though a spin−orbit or vibronic mechanism. The calculated energy of this band varies by 0.16 eV as a function of basis set and geometry and will be discussed in the next section.

Band 5. The fifth experimentally observed band is an $e \rightarrow d_{xy}$ ($^2E \leftarrow {}^2B_1$) allowed (in *x*,*y* polarization) charge transfer transition. The calculated energy of this band varies by 0.16 eV as a function of basis set and geometry.

(53) Swann, J.; Westmoreland, T. D. *Inorg. Chem.* **1997**, *36*, 5348−5357.

Band 6. The sixth calculated band is due to a second e → d_{xy} ($^2E \leftarrow {}^2B_1$) charge transfer transition, which is allowed in *x,y* polarization. The calculated energy of this band also varies up to 0.18 eV (Tables 4 and 5) and will be discussed in the next section.

Band 7. This band has been assigned as the third ligand field transition $d_{xy} \rightarrow d_{z^2}$ ($^2A_1 \leftarrow {}^2B_1$), which is symmetry forbidden in the C_{4v} point group, but its position was determined from the MCD experiments.[26] The calculated vertical excitation energy of this band is very sensitive to the starting geometry.

Bands 8 and 9. These bands are attributed to an $a_2 \rightarrow d_{xz,yz}$ ($^2E \leftarrow {}^2B_1$) transition, although experimentally (either by UV−vis or MCD spectroscopy) it is difficult to establish. In the present case, the calculated vertical excitation energies are found to be in the same region of bands 5 and 6. Because TDDFT calculations for the open-shell systems are conducted with unrestricted formalism, band 8 is assigned to the α set transition, while band 9 belongs to the β set transition (Figure S2).

Influence of the Experimental and Optimized Geometries on the Vertical Excitation Energies of $[MoOCl_4]^-$. The calculated vertical excitation energies for the first $d_{xy} \rightarrow d_{xz},d_{yz}$ ($^2E \leftarrow {}^2B_2$) ligand field transition is strongly dependent on the starting geometry (Tables 4 and 5, Figure S3). This transition differs for different geometries by ∼0.48 eV for both basis sets 1 and 4. A deviation of similar magnitude has been observed for the calculated vertical excitation energy for bands 8 and 9 (α and β set of $a_2 \rightarrow d_{xz,yz}$ ($^2E \leftarrow {}^2B_1$) transitions). Here, deviations of 0.48 and 0.52 eV for basis sets 1 and 4, respectively, are observed. The largest deviation in vertical excitation energies was observed for the $d_{xy} \rightarrow d_{z^2}$ ($^2A_1 \leftarrow {}^2B_1$) transitions (0.81 and 0.75 eV for basis set 1 and 4, respectively). For band 1, the calculated values (1.61−2.09 eV for basis set 1; 1.68−2.18 eV for basis set 4) are in reasonable agreement with the experimental value of 1.98 eV. The agreement is better for structures with a shorter Mo═O distance.[25]

The difference in the calculated vertical excitation energy for the second ligand field transition ($d_{xy} \rightarrow d_{x^2-y^2}$; $^2B_1 \leftarrow {}^2B_2$) is nearly half of the first ligand field transition (0.22 and 0.23 eV for basis set 1 and 4, respectively). Here, the calculated vertical excitation energy for all X-ray crystallographically derived geometries agrees well. In contrast, the $d_{xy} \rightarrow d_{z^2}$ ($^2A_1 \leftarrow {}^2B_1$) transition energy agrees with the experimental data only when the Mo═O distance is less than or equal to 1.61 Å. Interestingly, our model calculations (discussed in a following paragraph) indicate that the energy of the d_{z^2} orbital is very sensitive to the Mo═O bond distance. Finally, the calculated vertical excitation energies from a_2, b_1, and e orbitals to the d_{xy} orbital, i.e., charge transfer bands 3−6 ($a_2 \rightarrow d_{xy}$, $^2A_2 \leftarrow {}^2B_2$; $b_1 \rightarrow d_{xy}$, $^2B_2 \leftarrow {}^2B_1$; $e \rightarrow d_{xy}$, $^2E \leftarrow {}^2B_1$), are practically independent of the geometry (Tables 4 and 5). Among the geometries tested, the best agreement between the TDDFT results and the experimental data was observed for basis sets 1 and 4 with the structure with the CSD code TIXLIV (the MAD 0.13 eV and mean deviation 0.06 and −0.01 eV, respectively). Interestingly, the mean deviations and MAD values for both optimized geometries show slightly less than satisfactory agreement with the experimental data.

Table 6. Vertical Excitation Energies of the $[MoOCl_4]^-$ Core as a Function of the Mo═O Bond Length[a]

transition		calcd energy, eV, with each Mo═O distance						
composition[b]	excited state	1.60 Å	1.62 Å	1.64 Å	1.66 Å	1.68 Å	1.70 Å	1.72 Å
$d_{xy} \rightarrow d_{xz,yz}$	^2E	2.11	2.03	1.96	1.89	1.82	1.76	1.70
$d_{xy} \rightarrow d_{x^2-y^2}$	$^2B_1$	2.99	2.99	2.99	2.99	2.99	2.99	2.99
$d_{xy} \rightarrow d_{z^2}$	$^2A_1$	4.00	3.87	3.76	3.64	3.53	3.42	3.31
$2a_2 \rightarrow d_{xy}$	$^2A_2$	2.73	2.73	2.74	2.74	2.75	2.75	2.76
$11e \rightarrow d_{xy}$	^2E	3.34	3.34	3.34	3.34	3.34	3.34[d]	3.37[d]
$7b_1 \rightarrow d_{xy}$	$^2B_1$	3.38	3.38	3.39	3.39	3.40	3.40	3.40
$10e \rightarrow d_{xy}$	^2E	3.69	3.70	3.69	3.69	3.68	3.68	3.67
$2a_2$[c]$\rightarrow d_{xz,yz}$	^2E	3.75	3.67	3.60	3.53	3.46	3.41[d]	3.31[d]
$2a_2$[e]$\rightarrow d_{xz,yz}$	^2E	3.89	3.82	3.75	3.68	3.61	3.55	3.49

[a] Calculated using the TDDFT approach coupled with a uB3P86 exchange-correlation functional and basis set 4. [b] Predominant contribution: d_{xy} has $3b_2$ index, $d_{xz,yz}$ have 12e index, $d_{x^2-y^2}$ has $8b_1$ index, d_{z^2} has $13a_1$ index. [c] α set. [d] Strong mixing between $11e \rightarrow d_{xy}$ and $2a_2 \rightarrow d_{xz,yz}$ configurations. [e] β set.

Table 7. Vertical Excitation Energies of the $[MoOCl_4]^-$ Core as a Function of the O−Mo−Cl Angle[a]

transition		calcd energy, eV, with each O−Mo−Cl angle				
composition[b]	excited state	101°	102°	103°	104°	105°
$d_{xy} \rightarrow d_{xz,yz}$	^2E	1.65	1.71	1.77	1.83	1.89
$d_{xy} \rightarrow d_{x^2-y^2}$	$^2B_1$	3.05	3.03	3.02	3.00	2.98
$d_{xy} \rightarrow d_{z^2}$	$^2A_1$	3.57	3.58	3.59	3.59	3.59
$2a_2 \rightarrow d_{xy}$	$^2A_2$	2.81	2.80	2.78	2.76	2.73
$11e \rightarrow d_{xy}$	^2E	3.36	3.37	3.36	3.35	3.33
$7b_1 \rightarrow d_{xy}$	$^2B_1$	3.46	3.44	3.42	3.41	3.38
$10e \rightarrow d_{xy}$	^2E	3.64	3.65	3.67	3.68	3.68
$2a_2$[c]$\rightarrow d_{xz,yz}$	^2E	3.42	3.44	3.47	3.49	3.51
$2a_2$[d]$\rightarrow d_{xz,yz}$	^2E	3.53	3.57	3.60	3.63	3.66

[a] Calculated by using the TDDFT approach coupled with a uB3P86 exchange-correlation functional and basis set 4. [b] Predominant contribution: d_{xy} has a $3b_2$ index, $d_{xz,yz}$ have a 12e index, $d_{x^2-y^2}$ has a $8b_1$ index, d_{z^2} has a $13a_1$ index. [c] α set. [d] β set.

In order to understand the influence of the Mo═O distance and O−Mo−Cl angle on the vertical excitation energies, they were calculated for the model geometries where the Mo═O distance and O−Mo−Cl angle were changed with increments of 0.2 Å and 1°, respectively, keeping all other parameters invariant (Tables 6 and 7 and Figures 4 and 5). In the first set, where the Mo═O distance was altered, the four vertical excitation energies were significantly changed. These changes are related to a change in energy of the d_{z^2} and $d_{xz,yz}$ orbitals. The first transition is the $d_{xy} \rightarrow d_{xz},d_{yz}$ ($^2E \leftarrow {}^2B_2$) ligand field transition that primarily reflects a destabilization of the d_{xz},d_{yz} orbitals as a function of decreasing Mo═O distance. The transition energy change (0.41 eV) is comparable to the change in the energy difference between the d_{xy} and d_{xz},d_{yz} orbitals (0.43 eV). A similar magnitude of change was calculated for the vertical excitation energy in bands 8 and 9 (α and β set of $a_2 \rightarrow d_{xz},d_{yz}$ ($^2E \leftarrow {}^2B_2$) CT transition). Finally, the vertical excitation energy of the third ligand field transition, $d_{xy} \rightarrow d_{z^2}$ ($^2A_1 \leftarrow {}^2B_2$), should be dependent on the Mo═O distance as the d_{z^2} orbital energy is sensitive to the Mo═O distance. Because the energies of the d_{xy}, a_2, b_1, and e orbitals are practically invariant, little variation in CT transitions is observed for transitions involving these orbitals.

Table 8. Vertical Excitation Energies of the [MoOCl$_4$]$^-$ Core as a Function of the Basis Set[a]

transition		calcd energy, eV ($f \times 10^2$), with each basis set[b]					
composition[c]	excited state	none	d	2d	+	+, d	++, 2d, 2f
$d_{xy} \rightarrow d_{xz,yz}$	^2E	1.63 (0)	1.68 (0)	1.66 (0)	1.61 (0)	1.66 (0)	1.64 (0)
$d_{xy} \rightarrow d_{x^2-y^2}$	$^2B_1$	2.97 (0)	2.95 (0)	2.96 (0)	2.95 (0)	2.93 (0)	2.93 (0)
$d_{xy} \rightarrow d_{z^2}$	$^2A_1$	3.55 (0)	3.57 (0)	3.50 (0)	3.52 (0)	3.54 (0)	3.48 (0)
$2a_2 \rightarrow d_{xy}$	$^2A_2$	2.71 (0)	2.77 (0)	2.87 (0)	2.76 (0)	2.79 (0)	2.85 (0)
$11e \rightarrow d_{xy}$	^2E	3.30 (1.84)[f]	3.31 (1.56)	3.46 (0.88)[f]	3.34 (2.38)	3.38 (1.45)	3.43 (2.08)
$7b_1 \rightarrow d_{xy}$	$^2B_1$	3.33 (0)	3.39 (0)	3.51 (0)	3.39 (0)	3.42 (0)	3.49 (0)
$10e \rightarrow d_{xy}$	^2E	3.54 (0.03)	3.59 (0.03)	3.70 (0.03)	3.60 (0.04)	3.61 (0.03)	3.69 (0.04)
$2a_2{}^d \rightarrow d_{xz,yz}$	^2E	3.23 (0.48)[f]	3.38 (0.83)	3.40 (0.26)[f]	3.25 (0.17)	3.33 (1.18)	3.37 (0.47)
$2a_2{}^e \rightarrow d_{xz,yz}$	^2E	3.40 (0.06)	3.50 (0.05)	3.58 (0.04)	3.42 (0.03)	3.51 (0.03)	3.48 (0)
mean dev		0.25	0.21	0.17	0.22	0.20	0.18
MAD		0.28	0.25	0.25	0.27	0.25	0.26

[a] Calculated using the TDDFT approach coupled with a uB3P86 exchange-correlation functional and basis set 4 (crystallographically determined geometry with CSD code NABQIQ was used). [b] LANL2DZ ECP basis set was used for the molybdenum atom; for all other atoms, a 6-31G basis set with a number of diffuse (indicated as +) and polarization (indicated as d or f) functions was used. [c] Predominant contribution: d_{xy} has a $3b_2$ index, $d_{xz,yz}$ have a 12e index, $d_{x^2-y^2}$ has a $8b_1$ index, d_{z^2} has a $13a_1$ index. [d] α set. [e] β set. [f] Strong mixing between the $11e \rightarrow d_{xy}$ and $2a_2 \rightarrow d_{xz,yz}$ configurations.

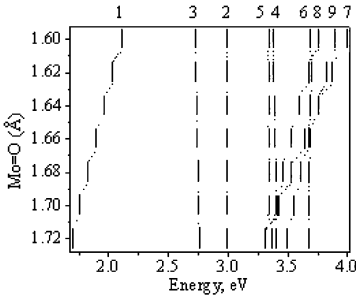

Figure 4. Vertical transition energies as a function of the Mo═O distance, calculated by the TDDFT approach. The B3P86 exchange correlation functional and basis set 4 were used.

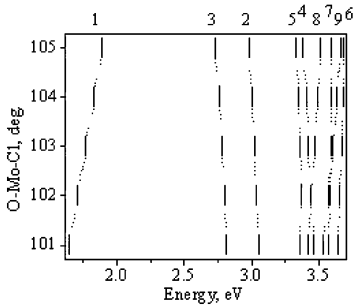

Figure 5. Vertical transition energies as a function of the O—Mo—Cl angle, calculated by the TDDFT approach using the B3P86 exchange correlation functional and basis set 4.

When the O—Mo—Cl angle is incrementally increased from 101° to 105°, the only $d_{xy} \rightarrow d_{xz},d_{yz}$ ($^2E \leftarrow {}^2B_2$) ligand field transition exhibited a significant change (0.24 eV, Table 7). Again, this change primarily reflects the destabilization of the d_{xz},d_{yz} orbital with a small concurrent stabilization of the d_{xy} orbitals. Indeed, a change in the transition energy of 0.24 eV is comparable to a 0.25 eV change in the energy difference between the d_{xy} and d_{xz},d_{yz} orbitals. The vertical excitation energy assigned to the α and β sets of $a_2 \rightarrow d_{xz,yz}$ ($^2E \leftarrow {}^2B_1$) transition changes by only 0.09 eV. Therefore, a shift toward higher energy is observed for both the first d—d transition (band 1) and the α and β sets of the $a_2 \rightarrow d_{xz,yz}$ ($^2E \leftarrow {}^2B_1$) transition (bands 8 and 9).

From these calculations, with different starting geometries of [MoOCl$_4$]$^-$, two important conclusions can be made. First, the excitations that involve the $d_{xz,yz}$ and the d_{z^2} orbitals are very sensitive to the Mo═O distance, while the O—Mo—Cl angle only significantly influences the $d_{xy} \rightarrow d_{xz},d_{yz}$ vertical excitation energy. Second, the calculated $a_2 \rightarrow d_{xz,yz}$ excitation energies of bands 8 and 9 in almost every geometry (except the geometries obtained from structures with CSD codes TIXLIV and PASCMO) are lower than the second $e \rightarrow d_{xy}$ transition (band 6). In other words, good agreement between the experimental and the calculated vertical excitation energies is observed only for relatively short Mo═O distances.

Influence of Exchange Correlation Functional and Basis Sets on the Calculated Vertical Excitation Energies. The dependence of vertical excitation energies on the exchange correlation functional was also investigated. First, all of the pure DFT exchange correlation functionals tested (BP86, BLYP, and BPW91), with a crystallographically determined starting geometry (CSD code NABQIQ), underestimate the vertical transition energies by at least 0.3 eV. As a result, the pure DFT methods were not examined any further. On the other hand, results from the hybrid DFT exchange correlation functionals (e.g., B3LYP and B3P86 calculations) are in better agreement with the experiments. This aspect was further probed by conducting six calculations on four starting geometries with two basis sets (basis set 1 and 4), and the results are presented in Table S6. Among the two hybrid functionals, the B3P86 yielded slightly better results than the B3LYP functional in terms of geometry and the vertical excitation energies. A similar conclusion was made for geometry optimization, thermodynamic, electronic structure, and the vertical excitation energy calculations in small organic molecules.[17,24,41,54]

In order to understand the influence of the basis set on the calculated vertical excitation energies, calculations with the NABQIQ starting geometry and basis sets 1—4 and 7—14 were conducted (Table 8). In contrast to diffuse function, addition of polarization function(s) to the 6-311G and 6-31G basis set improved the results. Indeed, the best results for the full electron basis, as well as effective core potential basis sets, were obtained by including two polarization functions.

(54) Kail, B.; Nemykin, V. N.; Davie, S. R.; Carrano, C. J.; Hammes, B.; Basu, P. *Inorg. Chem.* **2002**, *41*, 1281—1291.

The difference in the mean deviations and MAD for the calculated vertical excitation energies with larger basis sets and basis sets 1 or 4 (both with one polarization function) are very small. Here, inclusion of a single diffuse or polarization function resulted in only a small improvement in the predictive ability of the vertical excitation energies. As these transitions lie in the valence region, addition of a diffuse function resulted in only a very small improvement.[10,16,17,47]

4. Summary

The electronic structure and transition energies of the $[MoOCl_4]^-$ complexes have been calculated at different levels of theory with different geometries and basis sets. The semiempirical methods such as ZINDO and PM3 adequately described the occupied orbitals. However, both HF and MP2 gave wrong descriptions of the ground state. Electronic structure calculations suggest that the expected ordering of the metal centered orbitals can only be computed correctly by high-level DFT methods. The LF, as well as LMCT transition energies, of $[MoOCl_4]^-$ calculated by TDDFT method are in admirable agreement with the experimental electronic absorption and MCD spectra (with MAD of 0.13 eV). Among the exchange correlation functionals tested, the hybrid ones yielded better results. While inclusion of polarization functions in the basis set improved the results, the effect of inclusion of diffuse function is minimal. The calculated excitation energies are sensitive to Mo═O distance and O—Mo—Cl angle; the effect is prominent on $d_{xy} \rightarrow d_{xz,yz}$, $d_{xy} \rightarrow d_{z^2}$, and $a_2 \rightarrow d_{xz,yz}$ transitions. The results presented here clearly suggest that TDDFT is a powerful and viable approach for calculating the excited states in open shell, second row transition metal complexes.

Acknowledgment. Partial financial support from National Institute of Health, Grant GM 6155501, is gratefully acknowledged. We thank Mr. Brian Kail for helpful discussions.

Supporting Information Available: Additional figures and tables. This material is available free of charge via the Internet at http://pubs.acs.org.

IC0262942